

Optical Engineering

OpticalEngineering.SPIEDigitalLibrary.org

Alignment and assembly process for primary mirror subsystem of a spaceborne telescope

Wei-Cheng Lin
Shenq-Tsong Chang
Sheng-Hsiung Chang
Chen-Peng Chang
Yu-Chuan Lin
Chi-Chieh Chin
Hsu-Pin Pan
Ting-Ming Huang

Alignment and assembly process for primary mirror subsystem of a spaceborne telescope

Wei-Cheng Lin,^a Shenq-Tsong Chang,^{a,*} Sheng-Hsiung Chang,^b Chen-Peng Chang,^b Yu-Chuan Lin,^a Chi-Chieh Chin,^b Hsu-Pin Pan,^a and Ting-Ming Huang^a

^aInstrument Technology Research Center, National Applied Research Laboratories, 20 R&D Road VI, Hsinchu Science-Based Industrial Park, Hsinchu 300, Taiwan

^bNational Space Organization, National Applied Research Laboratories, 8F, 9 Prosperity 1st Road, Hsinchu Science-Based Industrial Park, Hsinchu 300, Taiwan

Abstract. In this study, a multispectral spaceborne Cassegrain telescope was developed. The telescope was equipped with a primary mirror with a 450-mm clear aperture composed of Zerodur and lightweighted at a ratio of approximately 50% to meet both thermal and mass requirements. Reducing the astigmatism was critical for this mirror. The astigmatism is caused by gravity effects, the bonding process, and deformation from mounting the main structure of the telescope (main plate). This article presents the primary mirror alignment, mechanical ground-supported equipment (MGSE), assembly process, and optical performance test used to assemble the primary mirror. A mechanical compensated shim is used as the interface between the bipod flexure and main plate. The shim was used to compensate for manufacturer errors found in components and differences between local coplanarity errors to prevent stress while the bipod flexure was screwed to the main plate. After primary mirror assembly, an optical performance test method called a bench test with an algorithm was used to analyze the astigmatism caused by the gravity effect and deformation from the mounting or supporter. The tolerance conditions for the primary mirror assembly require the astigmatism caused by gravity and mounting force deformation to be less than $P - V 0.02 \lambda$ at 632.8 nm. The results demonstrated that the designed MGSE used in the alignment and assembly processes met the critical requirements for the primary mirror assembly of the telescope. © The Authors. Published by SPIE under a Creative Commons Attribution 3.0 Unported License. Distribution or reproduction of this work in whole or in part requires full attribution of the original publication, including its DOI. [DOI: [10.1117/1.OE.54.11.115109](https://doi.org/10.1117/1.OE.54.11.115109)]

Keywords: Cassegrain telescope; primary mirror; bipod flexure; shim; coordinate measuring machine; astigmatism.

Paper 151271P received Sep. 20, 2015; accepted for publication Oct. 23, 2015; published online Nov. 18, 2015.

1 Introduction

A coordinate measuring machine (CMM) is a rapid, flexible, and capable tool, which can measure the dimensions, forms, and positions of geometric objects. It can also be used in optical assembly processes to compare the assembly result with the design tolerance. A typical CMM is composed of three orthogonal linear moving axes with a probe attached to the third moving axis, allowing a spherical stylus tip to conduct contact measurements on an object. Thus, the relative positions of the features that are in the reference frame of the machine and the reference frame based on the previously measured features of the object can also be calculated.¹ Certain tolerances of optomechanical subassemblies, such as the curvature radius, thickness, air space, decenter, axial translation, tilt, and roll,² can be derived by a precision CMM. Nevertheless, the surface accuracy of most critical optical components may be specified as $\lambda/20$ at 632.8 nm. Only interferometers or high-accuracy stylus profile meters are sufficiently accurate to meet the $\lambda/20$ measurement requirement.¹ However, a CMM is still useful for assessing the overall lens shape during manufacturing and at the acceptance phase, especially for large optical components. A Leitz CMM was used to develop the James Webb Space Telescope to control the radius of curvature, conic constant, and

aspheric figure for primary, secondary, and tertiary mirrors during generation and rough polishing. Moreover, CMMs are also used to assist the alignment of the primary mirror segment assembly to determine its contribution to the shim prescription in the James Webb Space Telescope.^{3,4} A high-precision CMM is a suitable tool for aiding the alignment of multiple elements in mid-size to large optical assemblies.

This study presents advanced techniques used for primary mirror assembly and the analysis of the bipod flexure bonding position. Lin et al. described the procedures for aligning primary mirrors and adjusting the isostatic mount to optimize the bonding position of Cassegrain telescopes by using a CMM. The method is a precise and useful method for aligning mid-size to large optomechanical systems.^{5,6} Kihm et al. proposed a novel design for adjustable bipod flexures used to mount mirrors and conduct optical experiments on a space telescope. The design reduced the error caused by the gravity effect to less than root mean square 10 nm.⁷ Lin et al. presented an optomechanical design and analysis method for a mirror mount integrated with a Cassegrain telescope. The deformation of the primary mirror caused by the gravity load from various mirror mounting positions can be predicted using finite element analysis (FEA) before primary mirror assembly.⁸ Moreover, lightweight spaceborne mirrors have large gravity sags and are difficult to operate, mount, and fix;⁹ thus, testing techniques could be challenges especially to verify the optical performance after a lightweight mirror is mounted. In developing the Kepler photometer, a

*Address all correspondence to: Shenq-Tsong Chang, E-mail: stc@itrc.narl.org.tw

counterweighted zero- g mount during the assembly process and a vertical setup were used for averaging up-and-down test results to predict zero- g effects. In the vertical setup, a mirror is used to minimize gravity effects by combining analytical FEA modeling of the gravity sag with interferometric test data to approximate a gravity-free surface figure.¹⁰ To specify the measured wavefront error contributed by manufacturing, gravity, and mounting force, Lin et al. proposed a novel method by using the characteristics of each Zernike term to obtain the absolute surface figure.¹¹

This article presents the alignment and assembly processes conducted using a high-performance CMM for a primary mirror. A mechanical shim was used to compensate for manufacturer errors present in components. Differences between local coplanarity errors and the bipod flexure bonding position during alignment were also measured. The thickness of the mechanical shim was determined using a CMM. The bipod flexures were bonded to the mirror by injecting epoxy after the flexures were bolted on the main plate to minimize the deformation of the surface shape. After primary mirror assembly, an algorithm based on Zernike coefficients was calculated using an optical test of the different orientations of the primary mirror was used to analyze the astigmatism caused by gravity and the deformation from the mounting or supporter. As a consequence, the astigmatism and trefoil aberration caused by the gravity effect and deformation of the mounting force were less than $P-V$ 0.02λ and $P-V$ 0.045λ at 632.8 nm , respectively. The results indicated that the mechanical ground-supported equipment (MGSE) designed for the alignment and assembly processes met the critical requirements for primary mirror assembly of the telescope.

2 Description of Optical System

The developed multispectral space telescope was a Cassegrain telescope with a 466-mm clear aperture and a 3600-mm effective focal length. To correct the field curvature, the correct lens was included. To account for the self-weight deformation and thermal distortion, the primary mirror was composed of Zerodur[®], and the lightweight scheme adopted a hexagon cell structure with a lightweight ratio of approximately 50%. The correct lens was composed of fused silica, and the truss, baffle, and main plate were composed of carbon-fiber-reinforced plastic, but the material used for the interface between the glass and the mechanical components (such as the bipod flexure, M2 fitting, correct lens cell, and housing) was invar. The system overview and lightweight scheme of the primary mirror (M1) are shown in Fig. 1. The figure shows that 60 deg of symmetry can be observed.

3 Design Concept of the Adjusting Mechanical Ground-Supported Equipment

3.1 Design Concept of the Adjusting Mechanical Ground-Supported Equipment of Primary Mirror

MGSE with a minimum of five degrees of freedom was required during the alignment of the primary mirror. The MGSE consisted of the main plate hanging MGSE, a main plate hanging MGSE supporter, and an M1 posture adjustment MGSE, as shown in Fig. 2. The main plate hanging MGSE served two main purposes: to transfer the reference plane on the back of the main plate and to provide a

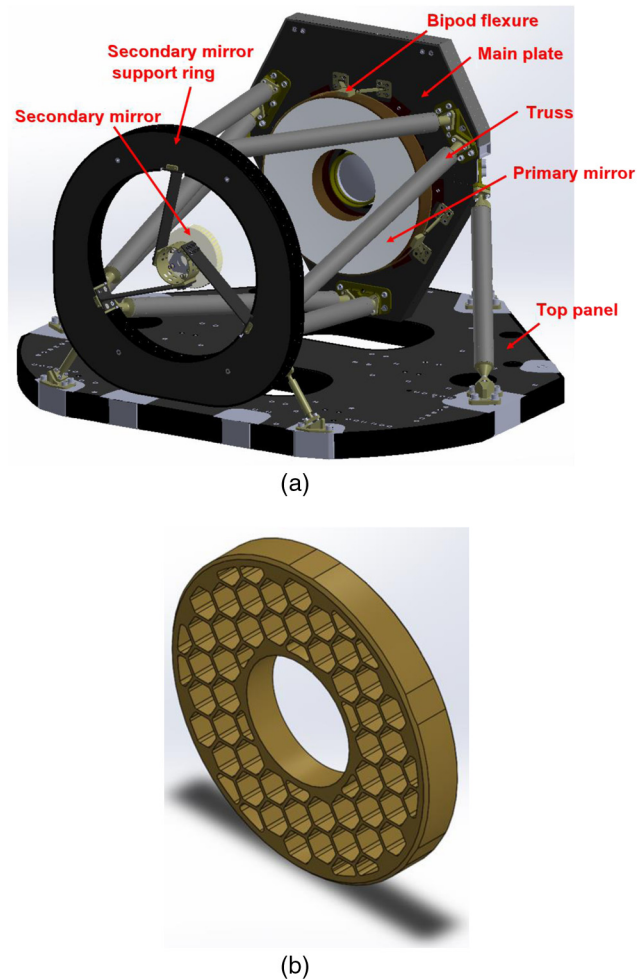
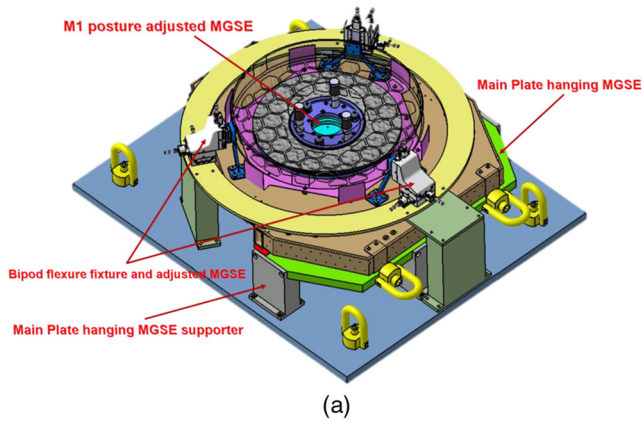


Fig. 1 System overview and lightweight scheme of the primary mirror of the multispectral telescope. (a) Schematic drawing of the Cassegrain telescope. (b) Lightweight scheme of the primary mirror.

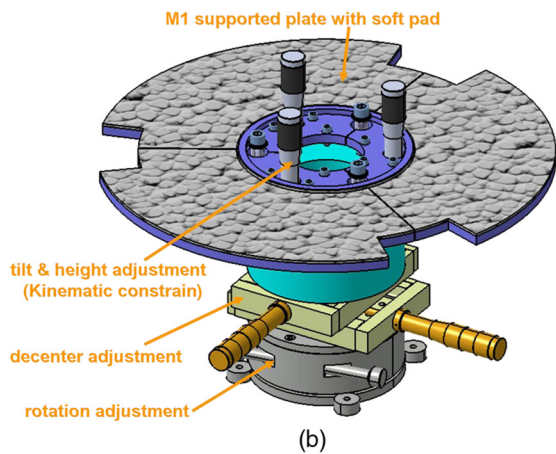
hanging function during the assembly and performance test. The M1 adjustment MGSE consisted of two linear translation stages, one rotation stage and one kinematic constraint platform, which fulfilled the following functions: decentering, orientating, and tilt and height adjustment of the posture of M1 relative to the main plate. M1 was placed on the steel-supported plate, and a soft pad was used as the interface between M1 and the supporting plate to reduce local stress caused by the unevenness of the supported plate. The adjusting mechanism of the M1 posture adjustment MGSE is shown in Fig. 2(b). The adjusted range of each accuracy screw on the tilt platform was calculated by analyzing the error compensation base of the position on the allocation of each accuracy screw.

3.2 Design Concept of the Adjusting Mechanical Ground-Supported Equipment of Bipod Flexure

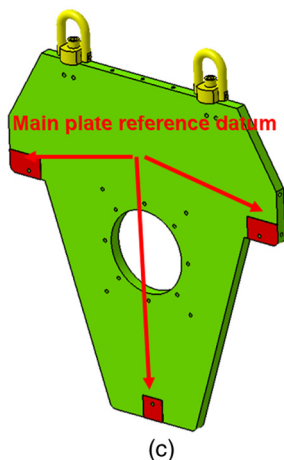
The outer diameter of the primary mirror exhibited six flat surfaces that were used as bipod flexure bonding areas. The bipod flexure bonding MGSE consisted of a bipod flexure fixture and the adjusting MGSE. The bipod flexure was mounted to the fixture by using three screws and assembled with the adjusting MGSE by using four screw-spring subassemblies to ensure that the bipod flexure exhibited the



(a)



(b)



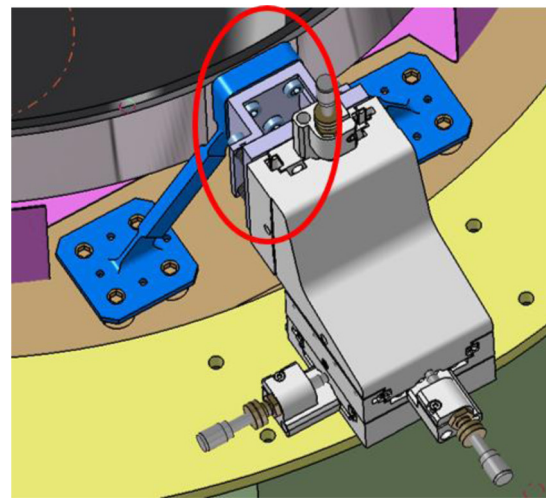
(c)

Fig. 2 Schematic drawing of the adjustment mechanism of the mechanical ground-supported equipment (MGSE) in the M1 assembly process. (a) System overview of M1, bipod flexure, main plate, and corresponding MGSE. (b) Mechanism of M1 posture adjustment MGSE. (c) Alignment datum on main plate hanging MGSE supporter.

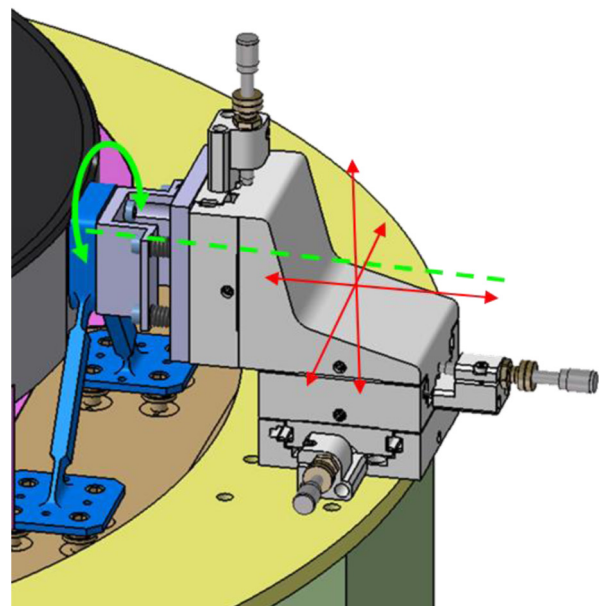
correct posture and controlled the bond line between M1. The bipod flexure adjusting MGSE was assembled with a three-axis translation stage as shown in Fig. 3.

3.3 Alignment Procedure for the Primary Mirror and Bipod Flexure

In general, the accuracy of the CMM is determined by the measurement scale of the machine. The accuracy of the Leitz PMM-F CMM, which was used in this study, was



(a)



(b)

Fig. 3 Adjustment mechanism of bipod flexure bonding MGSE. (a) Components of bipod flexure fixture and adjusting MGSE. (b) Concept of bipod flexure adjusting MGSE.

$2.3 + (1/400) * L \mu\text{m}$, where L is the length measured in millimeters. Before the M1 assembly, the manufacturer errors such as dimension and planarity errors of the bipod flexure and main plate shall be measured by CMM. As the manufactured error was known, the description of a mechanical compensated shim between the bipod flexure and main plate can be estimated before M1 assembly. This section states the preparation of the mechanical shim, the alignment procedure of M1, and the bonding procedure of bipod flexure (as shown in Fig. 4).

3.4 Description of Compensated Shim

To compensate for the astigmatism caused by deformation of the lightweight mirror because of gravity, the center of mass of the bonding pad of the bipod flexure was targeted to coincide with the plane through the center of gravity of the mirror (known as the neutral plane). To achieve this

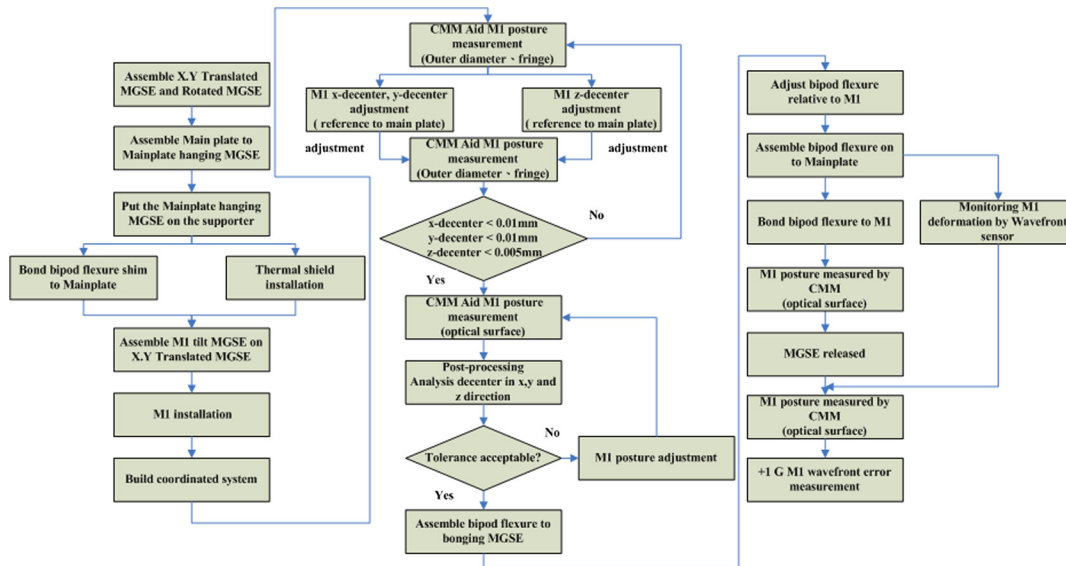


Fig. 4 Flowchart of the M1 alignment and the bipod flexure bonding procedure.

goal, the posture of the bipod flexure relative to the main plate was measured using a high-precision CMM. The mechanical shim was the interface between the bipod flexure and the main plate to compensate for manufacturer errors that occurred in each component and for the differences between the local coplanarity errors that occurred during alignment. The mechanical shim used in this process could be separated into two parts: the solid shim, which adjusted the bonding area of the bipod flexure to coincide with the neutral plane of the mirror, and the 0.01-mm-thick shim rings, which compensated for manufacturer errors and local coplanarity errors between the solid shim and base-plate of the bipod flexure. The solid shim was composed of invar to prevent a mismatch of the bipod flexure thermal expansion. The parameters of the shim rings were determined and calculated according to the dimensions of the bipod flexure, the thickness of the solid shim, and the distance from the bonding area of the main plate to the reference on the back of the main plane measured by the CMM. As shown in Table 1, B1 to B24 represent each interface of the thread inserts of the main plate with respect to each bipod flexure. With the measured thickness of the solid shim, bipod flexure dimension, and target height of the bipod flexure relative to the main plate, the thickness of the shim ring (shown in the “Thickness of compensated shim” column in Table 1) was easily calculated before bipod flexure installation. Table 1 shows that the deviation of the target value from the reference plate of the main plate to the solid shim was less than 0.008 mm.

3.5 Procedure for Aligning the Primary Mirror and Bipod Flexure to the Main Plate

The posture of the primary mirror was determined by the optical axis rather than the geometry of the primary mirror. A Leitz PMM-F 30.20.16 CMM was used to measure the profile of the optical surface and the coordinations of the contacted point measurement were then used to fit the radius, conic constant, and the posture parameters based on the least square fitting. Thus, decenter and tilt relative to the main plate were also analyzed using the macro developed by

the optical design software.¹² The M1 alignment procedure is shown in Fig. 5.

After completing the rough alignment, the fine alignment was based on the foundation of the optical surface measurement of M1 conducted by the CMM. The layout of the measured point scheme was separated into 10 zones with an equal arc length from point to point in each zone. After measurement, the contact point coordinate simulated by the CMM was exported as a .txt file, and then the real contact point coordinate can be compensated by a novel method with the ray trace foundation on the optical software. Based on the compensated data, the optical surface parameter of the measurement was analyzed using the x -decenter, y -decenter, z -decenter, and radius results produced by the optimization of the optical software. In this method, the conic constant is usually fixed, and the tilt is contributed as decenter. According to the analyzed posture, the three high-resolution screws adjusted the tilt less than 0.002 deg. The optimal bonding position with minimal astigmatism of the primary mirror caused by the gravity effect was simulated using the finite element method. The position of the bipod flexure was measured by the CMM and aligned to the correct position with an error of less than 0.01 mm in the axial and lateral positions. The bipod flexure was then integrated onto the main plate by using a torque wrench accompanied by strain gauge monitoring to measure any abnormal deviations. Figure 6 illustrates the status of the primary mirror alignment process by using CMM.

3.6 Bonding Process for the Bipod Flexure

After using bond line control to conduct fine alignment of the primary mirror and bipod flexure, 3M EC 2216 adhesive was injected into the gap between the mirror and bipod flexure. Before adhesive injection, treatments to prevent pollution of the optical surface and bipod flexure were performed. The bonding surfaces of M1 and the bipod flexure were carefully cleaned, and primers were painted on the bonding surfaces of the primary mirror and bipod flexure to maintain a bonding force. A dental mirror was used to ensure that the gap was completely filled with adhesive. A wavefront sensor

Table 1 Description of the mechanical compensated shim and estimated height of bipod flexure relative to main plate.

		No. insert	Height of solid shim (mm)	Bipod flexure height (mm)	Thickness of compensated shim (mm)	Compensated height of solid shim				
						Z (mm)	PA_PXPZ (deg)	PA_PYPZ (deg)	Div. (mm)	Parallelism
Bipod flexure III	Interface 1	B1	63.827	94.959	0.801	63.820	90.030	90.000	-0.007	0.076
		B2	63.827		0.806					
		B3	63.827		0.767					
		B4	63.827		0.779					
	Interface 2	B5	63.801	94.985	0.804	63.799	89.990	89.994	-0.002	
		B6	63.801		0.801					
		B7	63.801		0.766					
		B8	63.801		0.788					
Bipod flexure I	Interface 3	B9	63.823	94.963	0.556	63.824	89.992	90.011	0.001	0.007
		B10	63.823		0.555					
		B11	63.823		0.539					
		B12	63.823		0.548					
	Interface 4	B13	63.821	94.965	0.530	63.816	89.996	90.013	-0.005	
		B14	63.821		0.542					
		B15	63.821		0.533					
		B16	63.821		0.547					
Bipod flexure II	Interface 5	B17	63.798	94.988	0.603	63.792	90.002	89.976	-0.006	0.136
		B18	63.798		0.582					
		B19	63.798		0.604					
		B20	63.798		0.582					
	Interface 6	B21	63.795	94.991	0.522	63.802	89.953	90.045	0.007	
		B22	63.795		0.502					
		B23	63.795		0.529					
		B24	63.795		0.510					

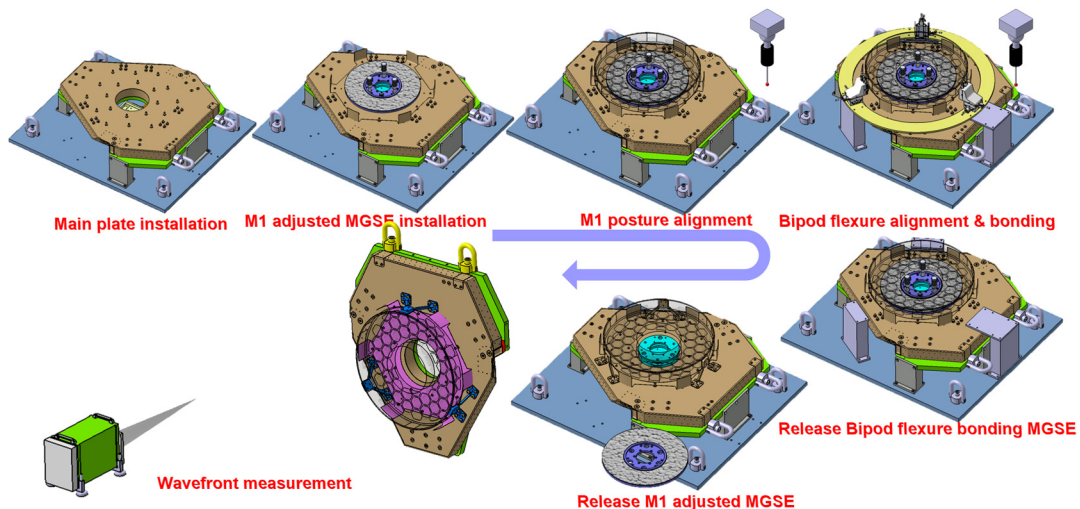


Fig. 5 Schematic drawing of the M1 alignment and the bipod flexure bonding procedure.

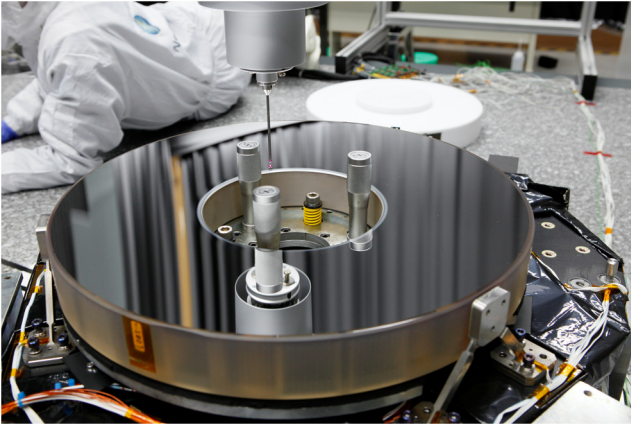


Fig. 6 Status of alignment process for the primary mirror by using coordinate measuring machine (CMM).

measurement system (wavefront sensor with an autocollimator and a compatible focusing module) and strain gauge were used to monitor the wavefront and strain variation while the adhesive cured, as shown in Fig. 7. Figure 8 illustrates the relative measurement during wavefront error monitoring, and Fig. 8(b) is the wavefront map subtracted from the map from Fig. 8(a) as the zero point before monitoring. Figure 8(c) shows the wavefront error deviation after EC 2216 was cured after 120 h. Figure 9–12 is the comparison of the wavefront deviation of the specified Zernike coefficient

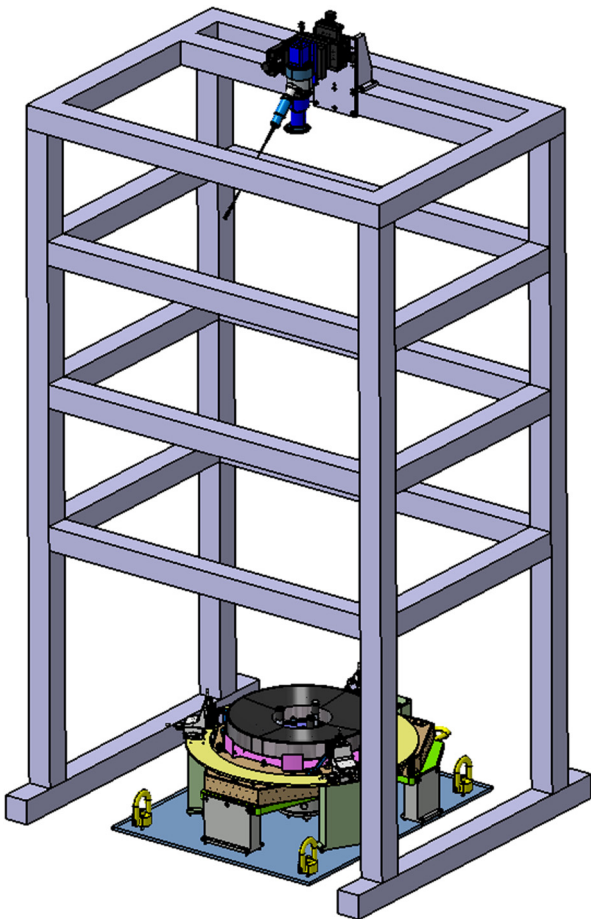
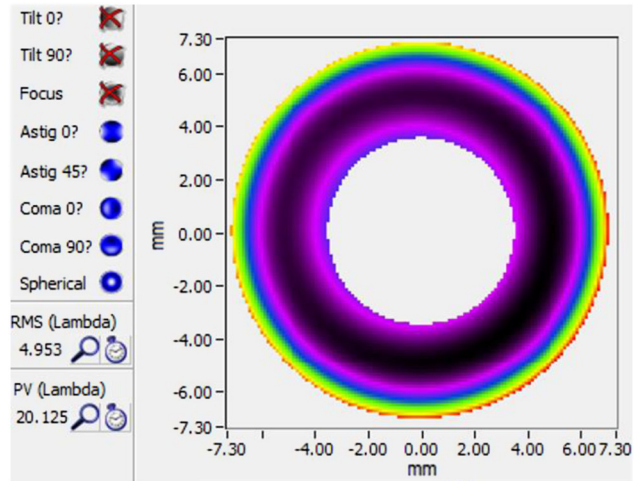
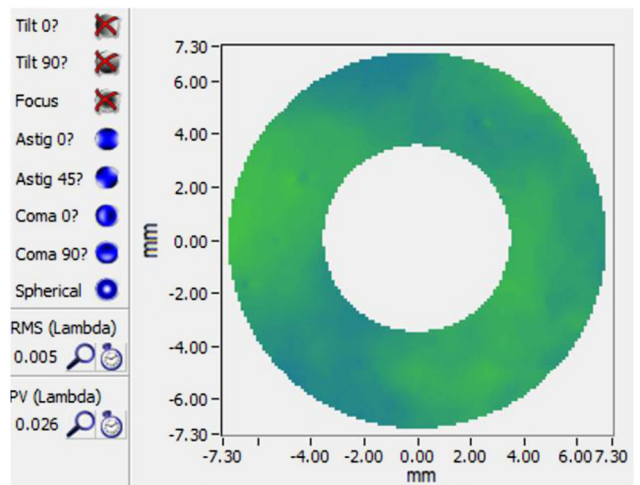


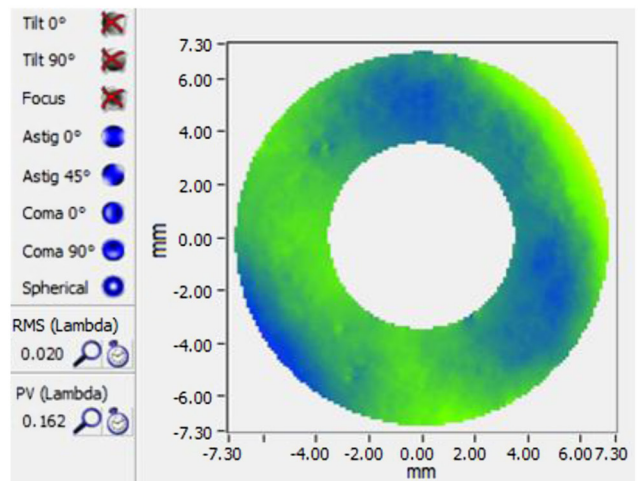
Fig. 7 Illustrations of experimental setup for wavefront sensor monitoring after EC 2216 injection in bipod flexure bonding process.



(a)



(b)



(c)

Fig. 8 Wavefront error map of wavefront sensor monitoring after EC 2216 injection process. (a) Wavefront error map of M1 measured by wavefront sensor. (b) Subtracted wavefront error as reference before monitoring. (c) Wavefront error deviation within 120 h.

when EC 2216 was cured for 132 h; it can be obviously found out that there was a slight trefoil caused from the shrinkage of the epoxy. Moreover, the induced coma may be contributed by misalignment from the wavefront sensor and primary mirror

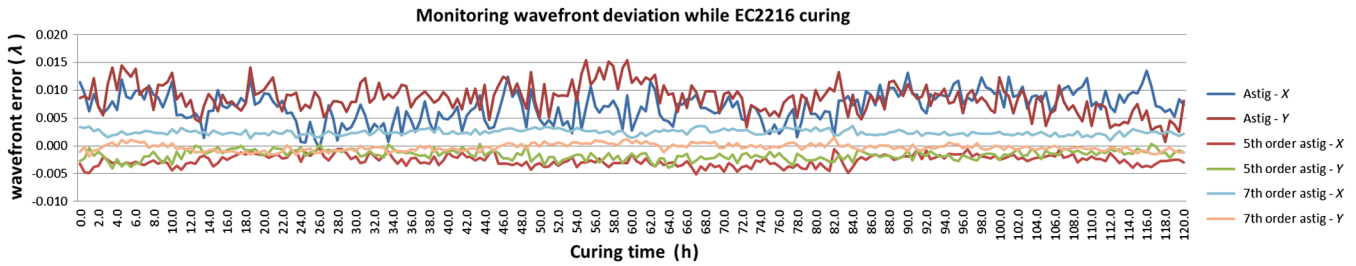


Fig. 9 Monitoring the astigmatism variation during the EC 2216 curing process within 120 h.

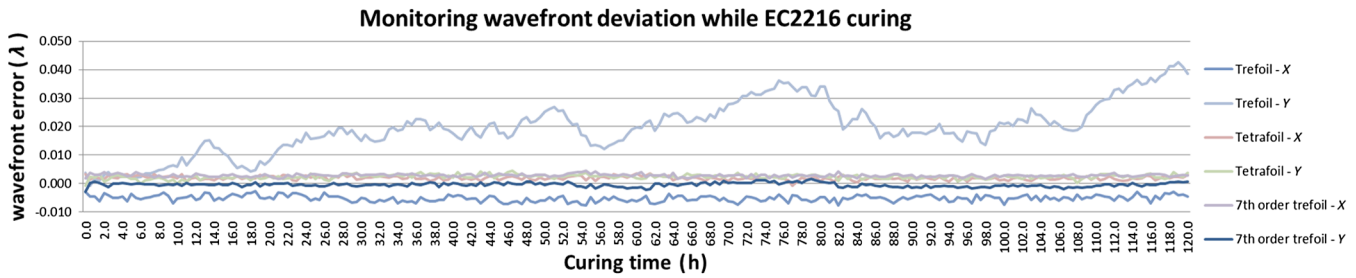


Fig. 10 Monitoring the trefoil variation during the EC 2216 curing process within 120 h.

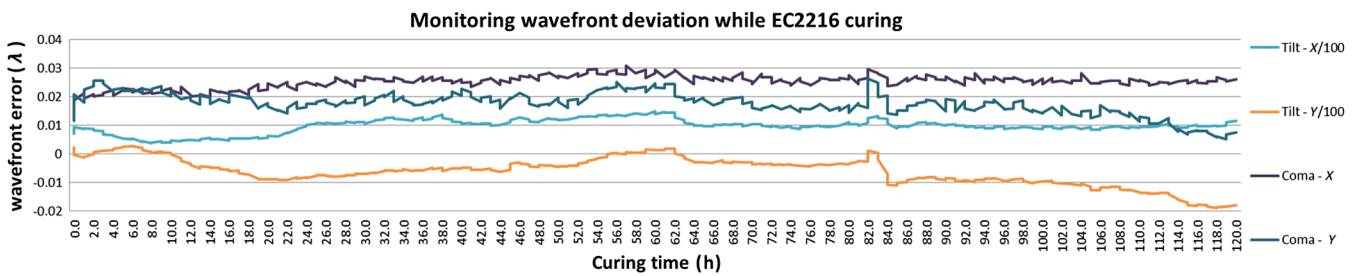


Fig. 11 Monitoring the coma and tilt variation during the EC 2216 curing process within 120 h.

	0	12 HR	Div.	120 HR	Div.	132 HR	Div.
Astig - X	0.012	0.005	-0.006	0.009	0.004	0.006	-0.003
Astig - Y	0.009	0.008	0.000	0.004	-0.004	0.023	0.019
Coma - X	0.014	0.021	0.007	0.026	0.005	0.028	0.002
Coma - Y	0.012	0.020	0.008	0.008	-0.012	0.018	0.010
3th order spherical aberration	0.009	0.014	0.005	0.013	-0.001	0.021	0.008
Trefoil - X	-0.003	-0.006	-0.003	-0.005	0.001	-0.008	-0.003
Trefoil - Y	0.004	0.010	0.007	0.035	0.025	0.034	-0.002
5th order astig - X	-0.003	-0.003	0.000	-0.003	0.000	-0.002	0.001
5th order astig - Y	-0.003	-0.001	0.001	-0.001	0.000	-0.004	-0.002
5th order coma - X	0.007	0.010	0.003	0.013	0.002	0.014	0.002
5th order coma - Y	-0.002	0.001	0.003	0.005	0.004	0.005	0.000
5th order spherical aberration	-0.002	-0.001	0.001	0.003	0.004	-0.006	-0.008
Tetrafoil - X	0.003	0.002	-0.001	0.002	0.000	0.003	0.001
Tetrafoil - Y	-0.001	0.003	0.004	0.002	-0.001	0.003	0.001

Fig. 12 Comparison of the wavefront variation during the EC 2216 curing process within 132 h.

caused from the displacement of the metrology frame due to thermal effects (as shown in Fig. 11).

4 Results and Discussion

4.1 Posture Deviation of the M1 and Bipod Flexure in Assembly Process

After the adhesive was completely cured, the M1 posture adjustment MGSE was disassembled. The CMM was

used to confirm the posture of M1 after the supporting MGSE was completely released. The changes in the posture of M1 and the bipod flexure are shown in Tables 2 and 3. Table 2 shows that even though the alignment error deviations of M1 and the bipod flexure were less than 0.005 mm in the alignment phase, a little movement was generated because the adhesive shrank during the curing and supporting MGSE removal phases. The deviation of the optical axis of the primary mirror was less than 0.004 deg. The

Table 2 Deviation of position of M1's posture during the bipod flexure bonding process.

	After fine alignment	Release bipod flexure mechanical ground-supported equipment (MGSE)	Gluing EC 2216	Release MGSE	Div.	Offset coordination	Div.
X-decenter	-0.0040	NA	0.0501	0.0491	-0.0010	-0.0009	-0.0009
Y-decenter	0.0002	NA	-0.0212	0.0162	0.0374	0.0047	0.0047
Z (mm)	147.9913	-0.0090	147.9933	147.9632	-0.0371	147.9616	-0.0387
Tilt-X (deg)	-0.0019	-0.0019	-0.0015	-0.0026	-0.0011	0.0022	0.0036
Tilt-Y (deg)	0.0003	0.0003	0.0019	0.0031	0.0013	0.0016	-0.0003
Rotated angle (deg)	179.9962	NA	179.9972	179.9972	-0.0028	0.0016	-0.0016

Table 3 Deviation of position of bipod flexure's posture during bonding process.

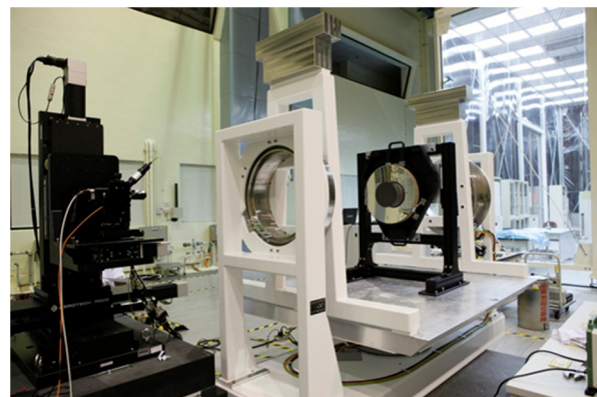
Unit (mm)	Distance from bipod flexure to M1 apex.				Div.
	Target value	Alignment level	After release MGSE	Offset coordination	
Bipod flexure No. 1	10.7657	10.7570	10.7574	10.7583	-0.0074
Bipod flexure No. 2	10.7657	10.7550	10.7609	10.7607	-0.0050
Bipod flexure No. 3	10.7657	10.7580	10.7638	10.7632	-0.0025

bonding position from the top surface of each bipod flexure relative to the apex of M1 during the whole bipod flexure bonding process is shown in Table 3. Deviation from the theoretical target value was maintained within 0.008 mm by using the alignment process and designed MGSE.

4.2 Optical Test with Wavefront Sensor

Wavefront measurement is an appropriate method for verifying whether the bipod flexure bonding process is suitable. A wavefront sensor with a 128×128 spatial resolution, auto-collimator, compatible focusing module, five-axis motorized stage system, and two-axis rotation gimbal were used during this step. Figure 13 shows the configuration of the setup for the optical performance test. The analysis method called a bench test was performed according to the characteristics of the Zernike polynomial. Although the measurement was conducted by a wavefront sensor, the results could also be output as fringe Zernike coefficients to identify the form error of the component or system aberrations. This method adopts the frequency of peaks and valleys of each fringe Zernike coefficient grabbed by the measurement with various orientations in a horizontal optical-axis configuration to separate the nonrotationally symmetric aberration of the mirror.¹² Based on the characteristics of each fringe Zernike term, the aberration from the residual form error after manufacturing was obtained before the bipod flexure bonding process. During the bench test, after the bipod flexure was bonded to the primary mirror, only form errors caused by manufacturing with mounting effects rotated as the mirror rotated, but the gravity effect and intrinsic systematic error did not. Therefore, the aberrations caused by the mount

($Aberration_{bond}$) can be obtained by the aberration with the mirror rotated ($Aberration_{rotated}$) minus the aberration from the manufacturing stage. The aberrations caused by the gravity effect could also be analyzed according to the symmetry of the lightweight scheme on the backside of the mirror with a period of 60 deg. Moreover, the intrinsic systematic error of the wavefront sensor can be determined as the bias of the overall bench test. The nonrotational Zernike coefficients of the various orientations of the primary mirror grabbed from the wavefront sensor can be plotted directly with a continuous curve as shown in Fig. 14. The rotational-symmetric aberration (spherical aberration) is nonsensitive for the gravity effect and mounting force; thus it can be neglected in this case.


Fig. 13 Experimental setup for the optical performance test after primary mirror assembly.

The posted analysis method for the absolute measurement is based on Zernike polynomials, which are an orthogonal set of polynomials with variables in radial, r , and azimuthal, θ , extent. A complete mathematical description for a given surface, $\Delta Z(r, \theta)$, is obtained by

$$\Delta Z(r, \theta) = A_{00} + \sum_{n=2}^{\infty} A_{n0} R_n^0(r) + \sum_{n=1}^{\infty} \sum_{m=1}^n R_n^m(r) [A_{nm} \cos(m\theta) + B_{nm} \sin(m\theta)]. \quad (1)$$

Each of the Zernike terms is a function of phase angle δ , such as tilt and astigmatism, and has a cosine and sinusoidal dependence, represented by the Zernike coefficients A and B , respectively. Each pair of terms may be expressed as a single term with an associated magnitude C and phase δ , expressed as follows:

$$C = \sqrt{A^2 + B^2}, \quad (2)$$

$$\delta = \frac{1}{m} \tan^{-1} \left(\frac{B}{A} \right). \quad (3)$$

Figure 14 shows the plotted curve for the astigmatism, trefoil, and tetrafoil terms. The obtained fringe Zernike coefficient with astigmatism terms of various orders consisted of the residual form error after manufacturing, mounting effect, gravity effect, and system calibration error. These errors meant that the characteristics of the measured astigmatism term were not exactly the same as the theoretical value, which was 180 deg. By contrast, the measured trefoil terms also consisted of the residual form error after manufacturing, mounting effect, gravity effect, and system calibration error, but the characteristics of the measured trefoil term were almost the same as the theoretical value, which was 120 deg. This phenomenon suggested that the form error

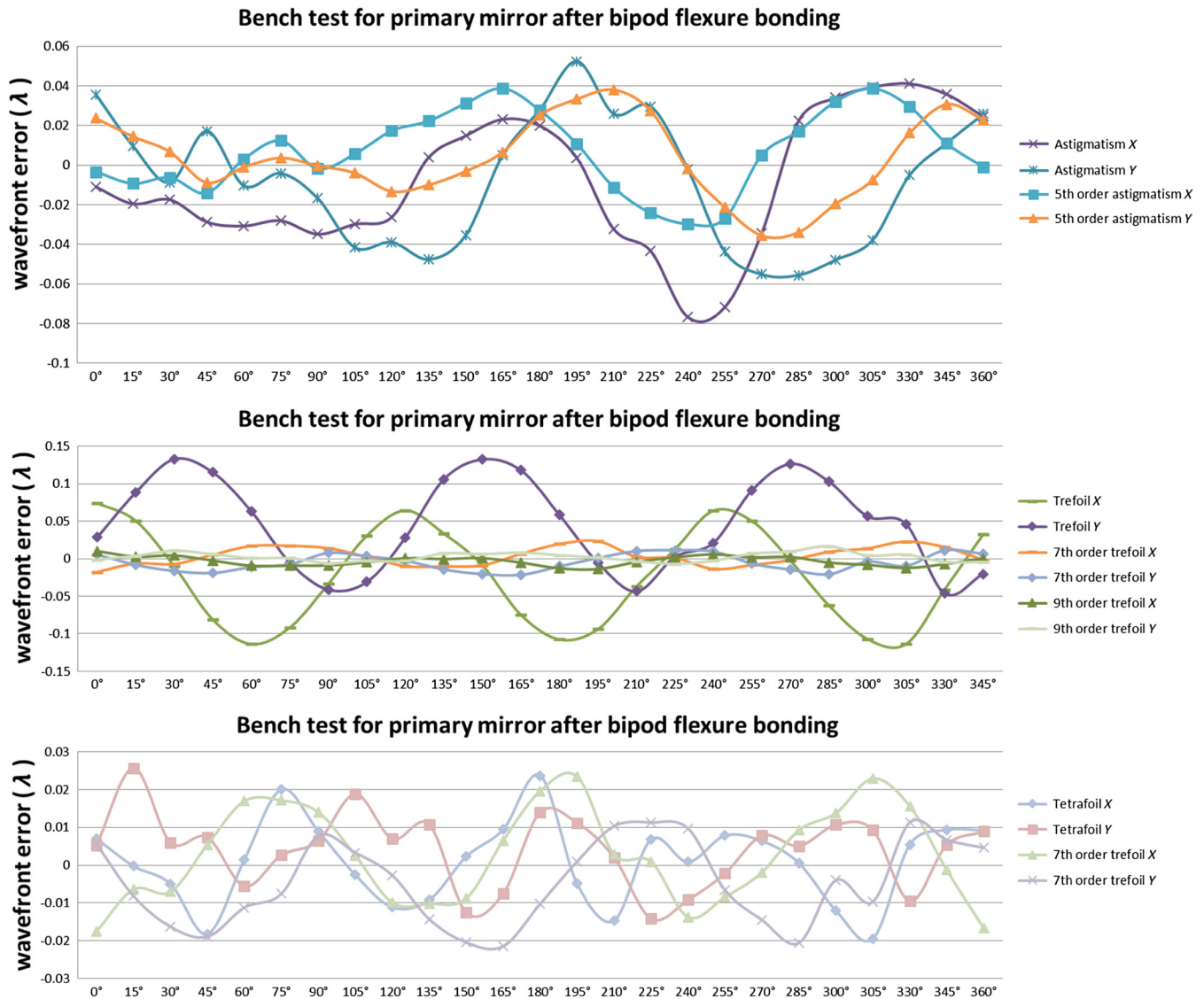


Fig. 14 Curve graph plotted by the Zernike coefficient gained from a bench test with different orientations of the primary mirror.

Table 4 Analyzed surface figure caused by manufacturer and deformation due to the mount and gravity effect.

Fringe Zernike coefficient		Aberration _{gravity}	Aberration _{constant}	Aberration _{rotated}	Aberration _{bond}
Magnitude (wave at 632.8 nm)	Pri astigmatism	0.019	0.014	0.040	0.016
	Pri coma	0.008	0.006	0.009	0.009
	Pri trefoil	0.008	0.052	0.085	0.044
	Sec astigmatism	0.015	0.007	0.023	0.030
	Sec coma	0.003	0.006	0.006	0.016
	Pri tetrafoil	0.003	0.004	0.012	0.017
	Sec trefoil	0.002	0.006	0.015	0.018
	Third astigmatism	0.006	0.011	0.009	0.008
	Phase (deg)	Pri astigmatism	-1.239	-18.954	66.798
Pri coma		52.634	37.502	-19.017	-19.017
Pri trefoil		-39.354	21.080	-56.544	-45.214
Sec astigmatism		2.488	78.559	53.787	46.847
Sec coma		19.831	-162.644	135.654	175.016
Pri tetrafoil		16.050	25.822	36.457	32.406
Sec trefoil		33.911	-42.313	10.122	19.364
Third astigmatism		-83.770	-3.705	-24.574	-37.497

with the mounting effect dominated the measured results and the trefoil was less sensitive to the gravity effect. According to the characteristics of the Zernike coefficient, the algorithm can be used to analyze the surface figure caused by intrinsic systematic error (Aberration_{constant}) and deformation caused by the mount (Aberration_{bond}) and gravity effects (Aberration_{gravity}). Table 4 shows a comparison of the measured results as fringe Zernike coefficients.

5 Conclusion

A CMM is an excellent tool to assist with aligning the primary mirror with respect to the main plate and aligning the bipod flexure to the correct bonding position. It can be obviously found that there was a slight trefoil with $P-V$ 0.034λ at 632.8 nm caused from the shrinkage of the EC 2216 cured for 132 h. Moreover, the aberration caused by the external force can be analyzed efficiently based on the theory of the bench test. As the final result, the designed MGSE successfully adjusted the posture of the primary mirror closed to the tolerance of the telescope. The bipod flexure was then bonded to the correct position to produce a small astigmatism aberration of $P-V$ 0.0188λ at 632.8 nm. This aberration was caused by gravity. The astigmatism aberration from mounting or bonding was approximately $P-V$ 0.0156λ at 632.8 nm. Moreover, the trefoil aberration due to the bond analyzed by the bench test is consistent with the monitoring wavefront deviation with the wavefront sensor. The above-mentioned result indicates that a suitable primary mirror assembly process minimized the astigmatism caused by the mounting effect.

References

1. E. F. Howick, D. Cochrane, and D. Meierc, "Using a co-ordinate measuring machine to align multiple element large optical systems," *Proc. SPIE* **6676**, 66760L (2007).
2. P. R. Yoder, *Opto-Mechanical Systems Design*, pp. 21–31, Marcel Dekker Inc., New York (1993).
3. H. P. Stahl et al., "Survey of interferometric techniques used to test JWST optical components," *Proc. SPIE* **7790**, 779002 (2010).
4. C. Wells et al., "Primary mirror segment assembly integration and alignment for the James Webb Space Telescope," *Proc. SPIE* **7793**, 779309 (2010).
5. W.-C. Lin et al., "The alignment of the aerospace Cassegrain telescope primary mirror and iso-static mount by using CMM," *Proc. SPIE* **8131**, 81310M (2011).
6. W.-C. Lin et al., "The alignment and iso-static mount bonding technique of the aerospace Cassegrain telescope primary mirror," *Proc. SPIE* **8491**, 84910M (2012).
7. H. Kihm et al., "Adjustable bipod flexures for mounting mirrors in a space telescope," *Appl. Opt.* **51**(32), 7776–7783 (2012).
8. Y. C. Lin et al., "Optimization and analysis of the primary mirror mounting position for Cassegrain telescope," in *Proc. 2012 Int. Conf. Convergence Information Technology (ICCIT 2012)*, *Lect. Notes Inf. Technol.*, Vol. **19**, pp. 53–58 (2012).
9. H. P. Stahl et al., "Design for an 8-meter monolithic UV/OIR space telescope," *Proc. SPIE* **7436**, 743609 (2009).
10. J. W. Zinn and G. W. Jones, "Kepler primary mirror assembly: FEA surface figure analyses and comparison to metrology," *Proc. SPIE* **6671**, 667105 (2007).
11. W.-C. Lin et al., "Comparing optical test methods for a lightweight primary mirror of a space-borne Cassegrain telescope," *Meas. Sci. Technol.* **25**, 094014 (2014).
12. S. T. Chang et al., "Measurement of radius of curvature by coordinate measurement machine," *Appl. Mech. Mater.* **284–287**, 488–492 (2013).

Wei-Cheng Lin is a PhD graduate student in the Department of Power Mechanical Engineering at the National Tsing Hua University. He is currently an associate engineer at the Instrument Technology Research Center, National Applied Research Laboratories. His research interests are optomechanical design, optomechanical system assembly, CMM measurement, and optical testing.

Sheng-Tsong Chang received his MS degree in physics from the Catholic University of America. He is currently an associated researcher at the Instrument Technology Research Center, National Applied Research Laboratories. His research interests are optical design, CMM measurement, optical testing, and performance evaluation of optical systems.

Sheng-Hsiung Chang is currently a vice technical engineer at the National Space Organization, National Applied Research Laboratories.

Chen-Peng Chang is currently a principal engineer at the National Space Organization, National Applied Research Laboratories.

Yu-Chuan Lin is a PhD graduate student in the Department of Engineering Science and Ocean Engineering at the National Taiwan University. He is currently an associate researcher at the Instrument

Technology Research Center, National Applied Research Laboratories. His research interests are optomechanical design and finite element analysis.

Chi-Chieh Chin is currently a vice technical engineer at the National Space Organization, and National Applied Research Laboratories.

Hsu-Pin Pan received his MS degree from the State University of New York, Buffalo. He is currently a researcher at the Instrument Technology Research Center, National Applied Research Laboratories.

Ting-Ming Huang received his PhD in aeronautics and astronautics from the National Cheng Kung University. He is currently a research fellow and division director at the Instrument Technology Research Center, National Applied Research Laboratories.